Mechanical Property of Pure Magnesium: From Orientation Perspective Pertaining to Deviation from Basal Orientation

S.K. Sahoo, R.K. Sabat, S. Panda, S.C. Mishra, and S. Suwas

Pure magnesium is subjected to cold rolling followed by annealing at 200 °C to obtain near-equiaxed grains of average grain size ~15 μm. The hardness of different grains/orientations of the annealed samples is estimated through consecutive characterization by nanoindentation and electron backscattered diffraction. It is observed that an increase in deviation from basal orientation decreases the hardness of an orientation. Orientations <14° from basal orientation have higher hardness compared to orientations at 14° to 28° from basal orientations. Subsequently, the texture and microstructure of pure magnesium are tailored to examine the correlation between volume fractions of basal orientations with the bulk hardness of the samples. A direct relationship of hardness with the volume fraction of basal orientations is observed. Magnesium with higher volume fraction of basal orientations has higher hardness.

1. Introduction

Magnesium and its alloys have a great potential for lightweight structural applications due to their low density and high specific strength (Ref 1). However, their poor formability at room temperature is an important limitation of magnesium for its usage as a structural material (Ref 2, 3). The development of strong basal texture during processing is responsible for this poor formability of magnesium (Ref 3–6). The main slip systems in magnesium are as follows: basal, $(0002)\langle 11\bar{2}0 \rangle$, prismatic, $(1\bar{1}00)\langle 11\bar{2}0 \rangle$, and pyramidal, $(11\bar{2}2)\langle 11\bar{2}3 \rangle$ slip systems (Ref 7–9). At room temperature, the critical reserved shear stress (CRSS) of basal slip systems shows much lower value than non-basal slip systems such as prismatic and pyramidal slip systems (Ref 10, 11). The basal slip systems cannot fully accommodate the external elongation, although tensile twinning offers lattice reorientation and further adjusts the degree of deformation at room temperature. With increase in temperature, the CRSS value quickly decreases for non-basal slip systems and activation of these slip systems improves the formability of magnesium (Ref 10, 11).

It has been attempted to deviate/alter the basal texture of magnesium through different processing techniques such as extrusion (Ref 12, 13), equal channel angular processing (Ref 14, 15), asymmetric rolling (Ref 16–18), thermo-mechanical processing (Ref 19, 20) etc., to improve its formability. In the present study, an attempt has been made to correlate the basal texture with mechanical property of pure magnesium. A fully recrystallized pure magnesium sample with average grain size of ~15 μm is subjected to nanoindentation for measurement of hardness corresponding to different grains/orientations. This has been achieved through consecutive characterization of nanoindentation and electron backscattered diffraction (EBSD). Subsequently, the texture and microstructure of pure magnesium have been tailored to examine the correlation between volume fraction of orientations and bulk hardness of pure magnesium.

2. Material and Methods

2.1 Material and Sample Preparation

Pure magnesium, obtained from General Motors, USA, is subjected to cold rolling of 90% reduction in thickness in a laboratory rolling mill. The rolled plates are then subsequently annealed at 200 °C for 5, 10, and 30 min, respectively. Both rolled and annealed samples are electro-polished for different characterizations. Electro-polishing is carried out using an electrolyte containing mixture of ethanol to ortho-phosphoric acid by 3:5 ratio (by volume) at 0 °C. Initially, the electro-polishing is carried out at 3 V for 30 s and subsequently at 1.5 V for 2 min. The nanoindentation is performed on the sample annealed for 30 min only. However, the samples annealed for 5 and 10 min of soaking time, respectively, are used to estimate a valuable correlation between volume fractions of basal orientations with the bulk hardness of the sample.

2.2 X-ray Diffraction (XRD)

XRD is carried out in a Bruker D8-Discover system using CuK$_\alpha$ radiation for both deformed and annealed samples. Six poles, (0002), $(10\bar{1}0)$, $(10\bar{1}1)$, $(10\bar{1}2)$, $(10\bar{1}3)$, and $(11\bar{2}0)$, are measured and are analyzed using a commercial software, Labotex 3.0 (Ref 21). Texture is measured on the ND plane containing RD-TD direction. The volume fraction of basal

S.K. Sahoo, S. Panda, and **S.C. Mishra**, Department of Metallurgical & Materials Engineering, NIT Rourkela, Rourkela 769008, India; and **R.K. Sabat** and **S. Suwas**, Department of Materials Engineering, IISc Bangalore, Bangalore 560012, India. Contact e-mail: sursahoo@gmail.com.
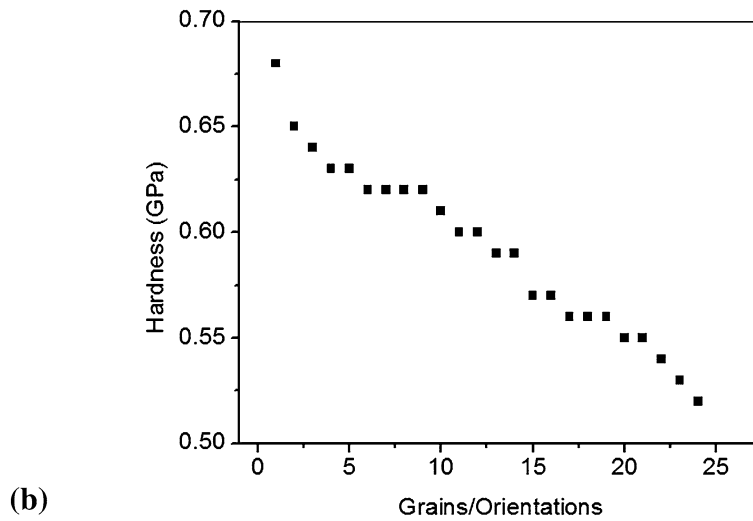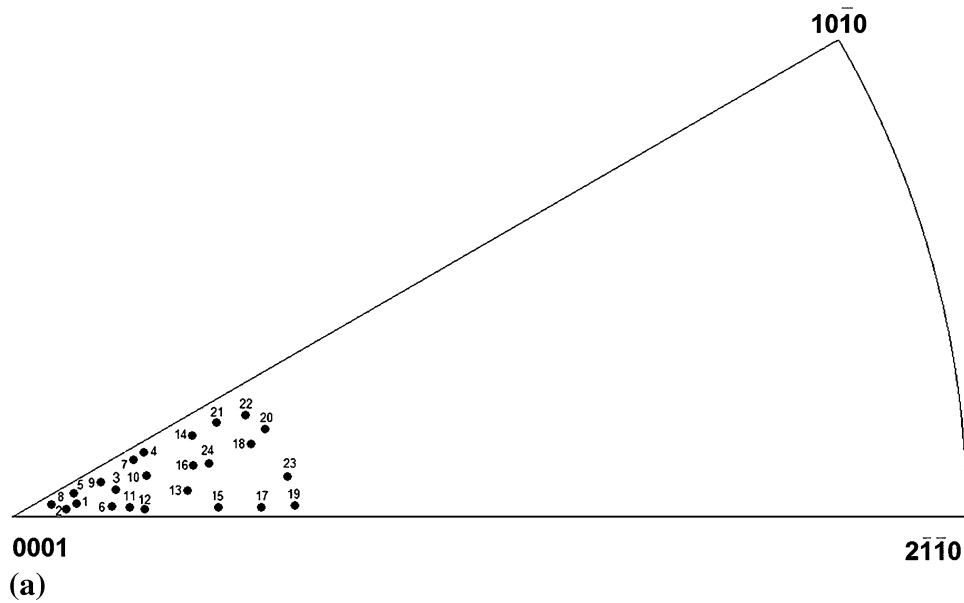
Fig. 1 (a) EBSD estimated discrete inverse pole figure representing the grains/orientations where nanoindentation is carried out; (b) Corresponding hardness of different grains/orientations shown in (a)

orientation is estimated through integration method where 15° tolerance from exact orientation is taken.

Dislocation density of basal, (0002), and off-basal, (01$\bar{1}$3), orientations is estimated through the methodology described in (Ref 22). The second order moment of the peak profile, $v_2(q)$ is related to the average dislocation density, $\langle \rho \rangle$ as follows:

$$v_2(q) = 2\Lambda \langle \rho \rangle \ln\left(\frac{q}{q_0}\right), \tag{Eq 1}$$

where $q = 4\pi \mathrm{Sin}\theta / 4\pi \mathrm{Sin}\theta \lambda . \lambda$, λ is the wavelength of the x-ray, and θ is half the Bragg angle. q_0 is a fitting parameter and Λ is a parameter that describes the dislocation contrast and is usually close to unity.

Stored energy values, for the basal and off-basal orientations, i.e., (0002) and (01$\bar{1}$3), respectively, are estimated using Stibitz formula (Ref 23):

$$\bar{E}_j(\alpha, \beta) = \frac{3}{2} Y_{hkl} \frac{(\Delta d/d)^2}{(1 + 2v_{hkl}^2)}, \tag{Eq 2}$$

where $\bar{E}_j(\alpha, \beta)$ is the stored energy and Y_{hkl} & v_{hkl} are the directionally dependent values of Young's modulus and Poisson's ratio. $\frac{\Delta d}{d}$ is obtained from the peak profiles as

$$\frac{\Delta d}{d} = \frac{B}{2 \tan \theta}, \tag{Eq 3}$$

and

$$B^2 = B_r^2 - B_a, \tag{Eq 4}$$

where B_r and B_a are the measured values of full width half maximum (FWHM) of the rolled and annealed samples, respectively.
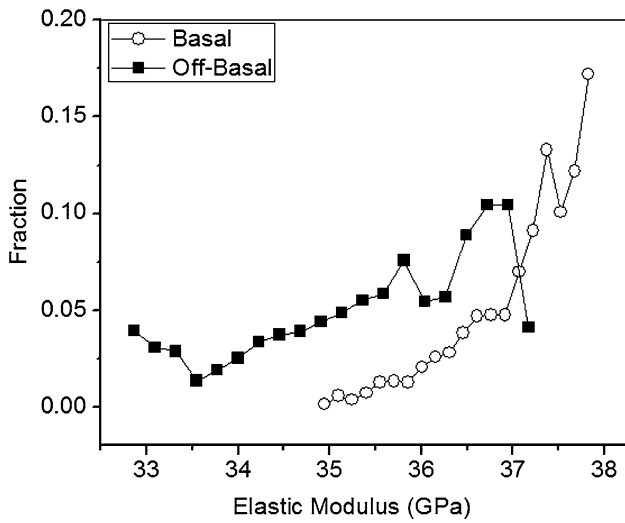
Fig. 2 Orientation estimated elastic modulus distribution of different grains/orientations of pure magnesium annealed at 200 °C for 30 min of soaking time. Basal orientations are those corresponding to <14° from exact basal orientation and off-basal orientations are 14° to 28° from exact basal orientation. In other words grains/orientations of 1 to 12 (Fig. 1a) are basal grains/orientations, whereas others, i.e., 13 to 24, are off-basal grains/orientations

2.3 Electron Backscattered Diffraction (EBSD)

EBSD, on the ND plane of the magnesium samples, is carried out on a FEI-Quanta 200-HV SEM (scanning electron microscope). Data acquisition and analyses are performed using the TSL-OIM version 6.0 software. Beam and video conditions are kept identical between the scans and a step size of 0.2 μm is used. Misorientation in a grain is represented by grain orientation spread (GOS) and it is defined as the misorientation between all measurement points of a grain and the grain average orientation. Orientation estimated elastic stiffness of different grains is estimated using the procedure explained elsewhere (Ref 24). Based on the known single-crystal elastic constants of hexagonal titanium, orientation information, and appropriate strain tensor, average polycrystalline elastic stiffness values are estimated using the Voight and Reuss averaging scheme (Ref 24) using TSL-OIM software. The deformation (strain) gradient used for the present study is as follows:
$\begin{bmatrix} -0.5 & 0 & 0 \\ 0 & -0.5 & 0 \\ 0 & 0 & 1 \end{bmatrix}$. Schmid factor (Ref 25) of different grains/orientations is determined using the basal slip system and the stress state as follows: $\begin{bmatrix} -0.5 & 0 & 0 \\ 0 & -0.5 & 0 \\ 0 & 0 & 1 \end{bmatrix}$.

2.4 Nanoindentation

Nanoindentation is carried out using a nanomechanical testing instrument, Hysitron Triboindenter (TI 900). A Berkovich diamond indenter is used for indentation. Hardness of approximately 50 grains on the ND plane is measured using a load of 11,000 μN.

2.5 Vickers Hardness

Vickers hardness is measured on the ND plane in a LECO Microhardness tester LM 248AT using 0.1 kgf load and a dwell
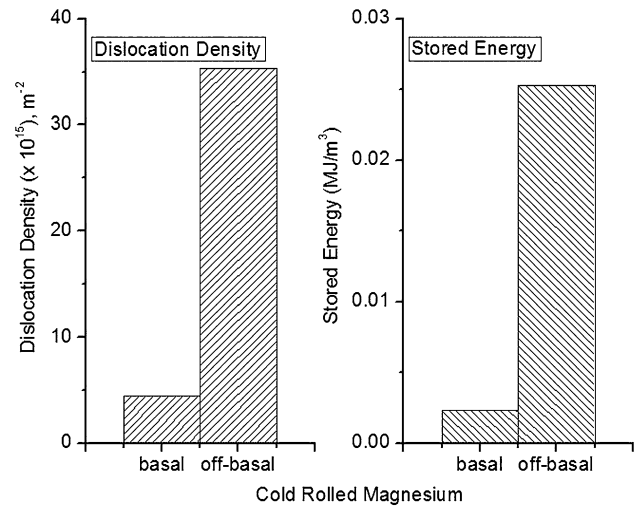
Fig. 3 XRD estimated dislocation density and stored energy w.r.t. different orientations in pure magnesium. Basal: (0002); Off-basal: (01 $\bar{1}$3)

time of 15 s. Average hardness of 10 indentations at different regions of the sample is estimated.

3. Results

Figure 1 shows the hardness of different grains/orientations of pure magnesium annealed at 200 °C for 30 min of soaking time. The discrete inverse pole figure shown in Fig. 1(a) is a representation of grains/orientations where nanoindentation has been carried out. The corresponding hardness of different grains/orientations is shown in Fig. 1(b). It may be observed from the figure that the hardness of grains/orientations decreases with increasing deviation from basal orientations. The grains away from basal orientations (>14° from exact basal orientation, i.e., grains/orientations numbered from 13 to 24) have relatively lower hardness values. Figure 2 shows the relative elastic modulus values, as estimated from EBSD analysis, of basal grains/orientations (<14° from exact basal orientation) and off-basal orientations (14° to 28° from exact basal orientation), respectively, of pure magnesium annealed at 200 °C for 30 min of soaking time. This is achieved by partitioning the EBSD scan into two parts, i.e., grains corresponding to basal orientations and those corresponding to off-basal orientations. However, this analysis has been performed with a separate EBSD scan obtained on another region of the sample—after knowing the nanohardness (Fig. 1a) values corresponding to different orientations. Figure 2 shows a higher value of elastic modulus for basal grains/orientations compared to off-basal grains/orientations. The XRD estimated dislocation density and stored energy of different orientations in pure magnesium before annealing, which is shown in Fig. 3. This shows a relatively lower value of dislocation density and stored energy for basal orientation compared to that for off-basal orientation, respectively. It may be noted that the sample annealed for 30 min of soaking time is used to estimate the instrumental effect on XRD peak profile and hence, the orientation effect on dislocation densities and stored energy values is estimated for rolled pure magnesium
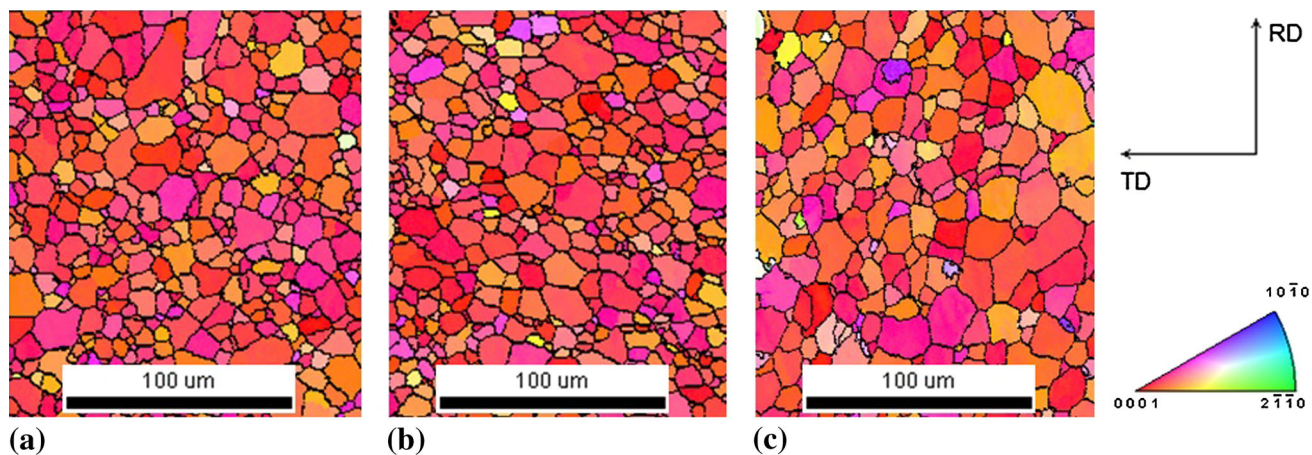
Fig. 4 IPF maps of magnesium samples annealed at 200 °C for different soaking times: (a) 5 min, (b) 10 min, and (c) 30 min
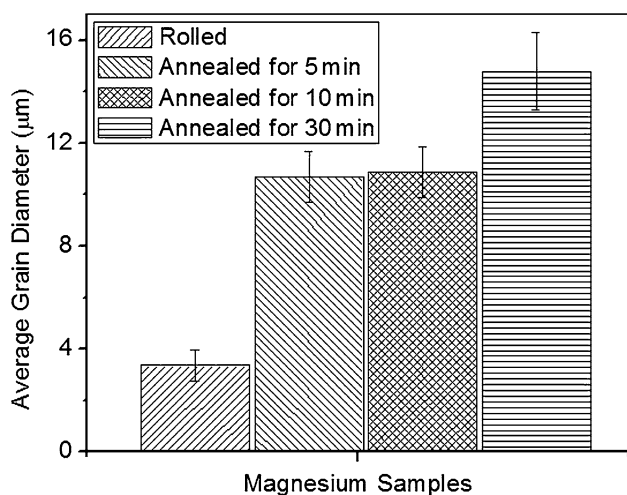
Fig. 5 Effect of grain size as a function of soaking time of annealing at 200 °C in pure magnesium

Fig. 6 Grain orientation spread (GOS) of pure magnesium samples annealed at 200 °C for 5 and 10 min of soaking time, respectively

sample only. It is apparent from Fig. 3 that the grains with off-basal orientations possess a higher amount of strain compared to basal-orientated grains.

Figure 4 shows the EBSD micrographs, in the form of inverse pole figure (IPF) maps, of samples annealed at 200 °C for different soaking times. The maps clearly show a dominant basal texture in the samples. It can also be seen from the figure that the samples are fully recrystallized after 5 min of soaking time and a significant grain growth can be observed in the sample annealed for 30 min. The average grain size as a function of soaking time of annealing is shown in Fig. 5. The samples annealed for 5 and 10 min of soaking time, respectively, show an insignificant grain growth during annealing. As shown in Fig. 6, the samples annealed for 5 and 10 min of soaking time, respectively, have also insignificant development of GOS during annealing.

The texture development, in terms of (0002) pole figure, during annealing of pure magnesium is shown in Fig. 7. The figure shows a decrease in basal texture when annealed for 5 min of soaking time which further increases on increasing the soaking time. The volume fraction of basal orientation as a

function of soaking time of annealing is presented in Fig. 8. Initially, the volume fraction drops at 5-min soaking time and then it increases with further increase in soaking time of annealing. It may be noted that pure magnesium is annealed at 200 °C for different soaking times varying from 30 s to 5 min and shows a decrease in basal texture as a function of soaking time of annealing.

The Vickers hardness of different magnesium samples is shown in Fig. 9. This shows a general decrease in Vickers hardness with progressive annealing. However, an increase in hardness value can be seen in the sample annealed for 10 min of soaking time.

4. Discussion

It has been reported that in hexagonal metals/alloys, the basal grains/orientations are harder compared to off-basal or non-basal grains/orientations (Ref 24, 26–28). In the present
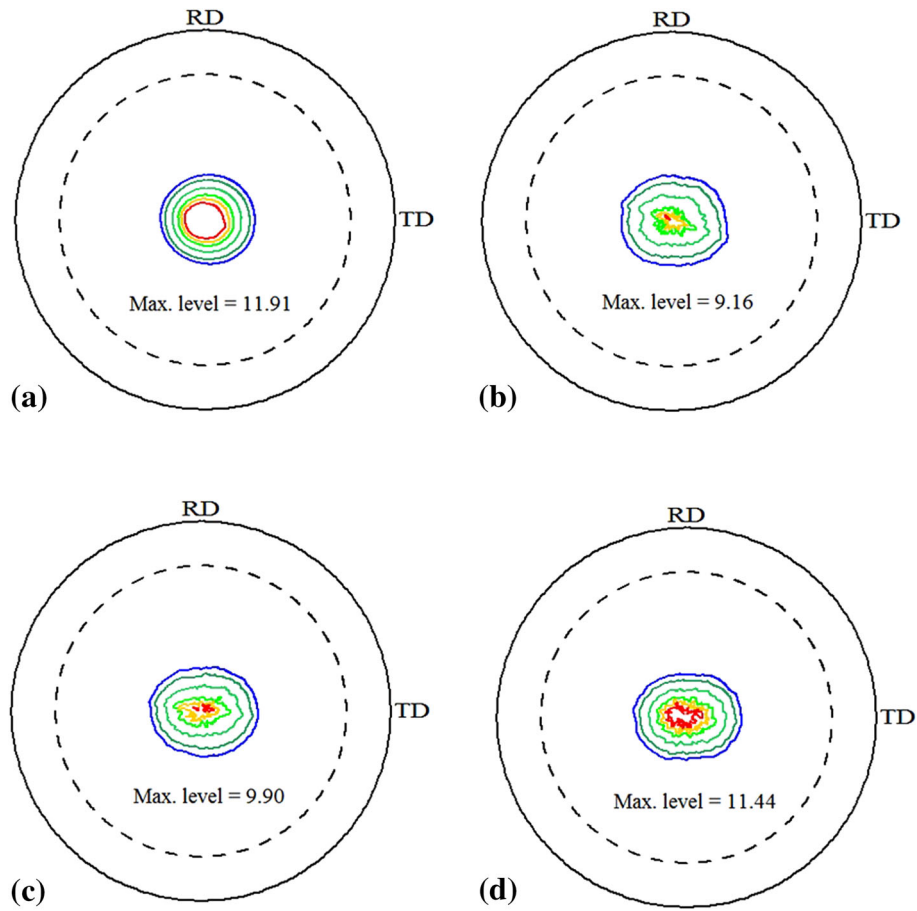
Fig. 7 (0002) pole figure of magnesium samples before and after annealing: (a) Cold rolled, (b) Annealed at 200 °C for 5 min, (c) Annealed at 200 °C for 10 min, and (d) Annealed at 200 °C for 30 min. The contour levels are at 2, 4, 6, 8, and 9 times random
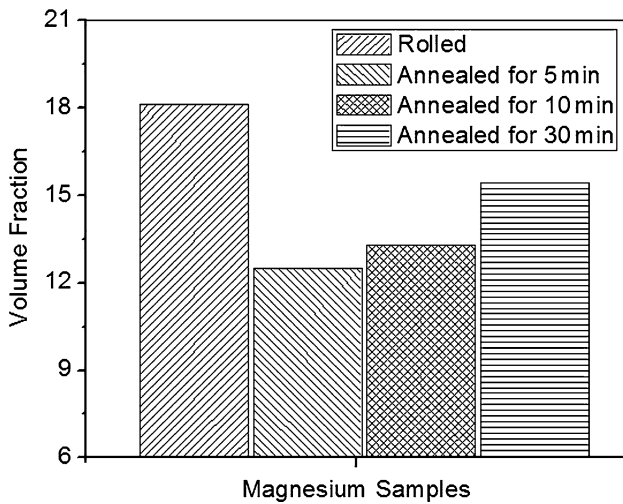
Fig. 8 Volume fraction of $(0001)\langle 10\bar{1}0\rangle$ orientation (i.e., basal orientation) in rolled and annealed pure magnesium samples
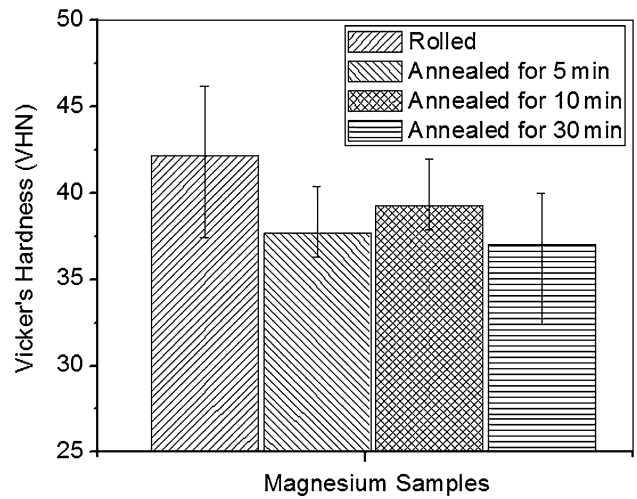
Fig. 9 Vickers hardness of pure magnesium samples before and after annealing

study, it has also been found that the orientation dependence of hardness in magnesium is not different from other hexagonal metals/alloys. The higher hardness of basal grains is in line with the findings of several researchers (Ref 29–31). For magnesium, the active slip systems at room temperature deformation are different from that of titanium/zirconium (Ref 7–9). Figure 10 shows a schematic for possible explanation of higher hardness pertaining to basal orientations in pure magnesium. Three possible orientations (represented by an unit cell) are shown in the figure: Figure 10(a) shows that *c*-axis of the unit
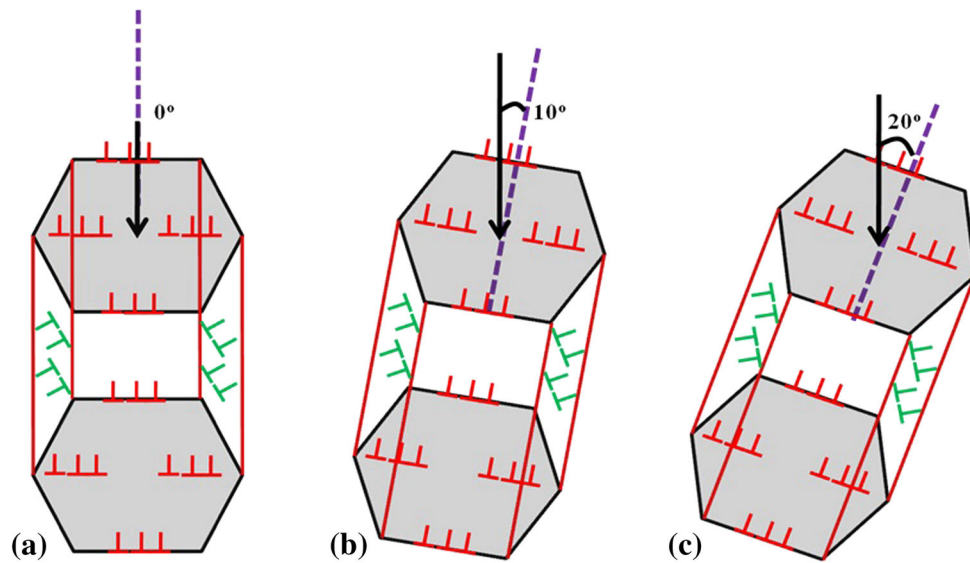
Fig. 10 Orientation (represented an unit cell) w.r.t. the direction of indentation: (a) *c*-axis of the unit cell is parallel to the indention direction, (b) *c*-axis of the unit cell is 10° to the indention direction, and (c) *c*-axis of the unit cell is 20° to the indention direction. Red color dislocations: basal dislocations and green color dislocations: prismatic dislocations (Color figure online)
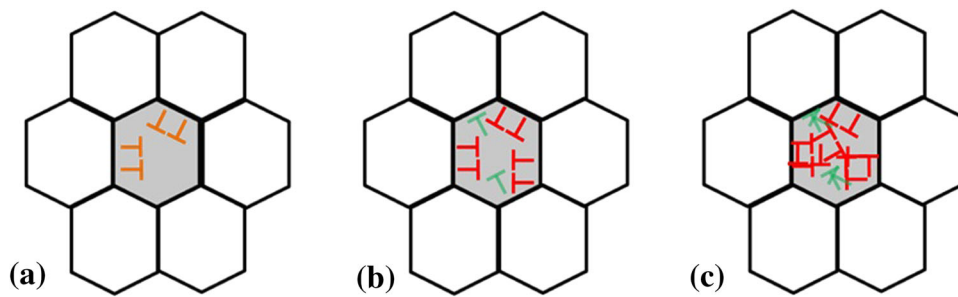
Fig. 11 Grains corresponding to the respective orientations shown in Figure 10. The grain with gray color is subjected to nanoindentation. Respective dislocation activations after nanoindentation are also shown in the schematic. Saffron color dislocations: pyramidal dislocations, Red color dislocations: basal dislocations and green color dislocations: prismatic dislocations (Color figure online)
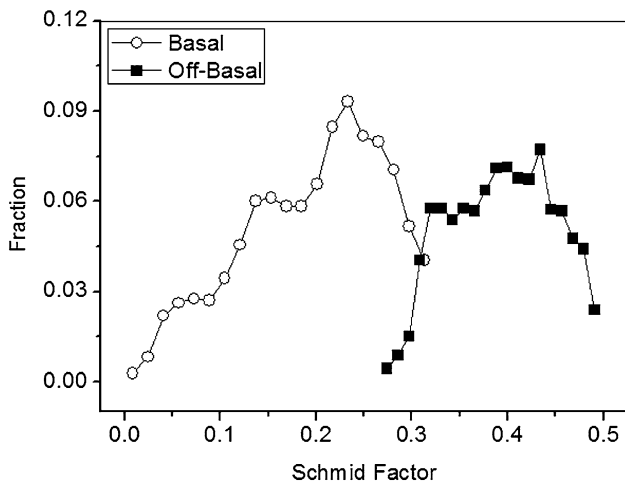
Fig. 12 Schmid factor distribution of basal and off-basal grains/ orientations of pure magnesium annealed at 200 °C for 30 min

cell is parallel to the indention direction, whereas Fig. 10(b) and (c) shows that the indentation direction is at 10° and 20° to the *c*-axis of the unit cell, respectively. Dislocations present in

the basal and prism planes are, respectively, represented by red and green color. It is well known that in magnesium, basal dislocations are easily activated than other dislocations because of low value of CRSS for basal slip. Hence it is expected that favorable orientation for basal slip is responsible for difference in the hardness of magnesium. The orientation shown in Fig. 10(a) is difficult to slip and expected to be harder orientation. The generation of contraction twins (Ref 32–35) can be expected in orientations where the indentation direction is parallel to *c*-axis of the orientation (i.e., in case of Fig. 10a). However, these twins are not observed in the present study. These twins, in any case, resist the indentation as they require higher stress to activate (Ref 33, 34). It may also easily be visible from Fig. 11, where a schematic shows the dislocation activities in grains w.r.t. the orientations presented in Fig. 10. In Fig. 11, the gray-colored grain is subjected to nanoindentation. It is expected that the grain whose *c*-axis is parallel to the indent axis (Fig. 11a) activates pyramidal slip after indentation. As the basal plane is perpendicular to the applied loading axis, neither prismatic nor basal slip system will active because the planes are generally parallel and perpendicular to the applied axis. Hence, there is the only possibility of activating contraction twin in the sample. Formation of contraction twin is associated

with the crack formation on the sample surface (Ref 33, 34), and after nanoindentation no such crack is observed on the sample surface which indicates that the deformation is associated with higher order slip systems namely pyramidal $\langle c + a \rangle$ type. As the CRSS required for pyramidal slip is more than basal slip (Ref 15, 36), a higher hardness value for these basal orientations is expected. However, in Fig. 11(b) and (c), the grains being favored with the slip directions, a relatively more dislocation activities may be observed in these grains. This has been also estimated in Fig. 3; a higher dislocation density for off-basal orientations. To evaluate further the Schmid factor, distribution of these two orientations, basal and off-basal, is estimated from EBSD analysis by partitioning the EBSD scan. The results of Schmid factor distribution are shown in Fig. 12. This clearly shows a lower distribution of Schmid factor for basal orientations indicating a higher strength of these orientations.

Other important finding in the present study is the correlation of volume fraction of basal orientation with bulk hardness of magnesium. As shown in Fig. 4, 5, and 6, samples annealed for 5 and 10 min of soaking time have approximately equal microstructural developments. Both grain size and GOS developments are insignificant in these samples. However, the texture development in these samples is quite different (Fig. 7 and 8). The decrease in basal texture during annealing for 5 min could be due to lower stored energy of basal orientation (Fig. 3). However, the increase in basal texture on further annealing (10 min) may be attributed from the end of recrystallization or beginning of grain growth phenomena. As the basal texture of both the annealed samples is different, it may not be improper to correlate texture of these samples with their mechanical properties. It may be noted that the correlation of bulk mechanical property of magnesium is limited to Vickers hardness. This is because very smaller pieces of pure magnesium samples are obtained after 90% of rolling. It has been observed that the sample annealed for 10 min of soaking time, i.e., the sample having higher volume fraction of basal orientations, has higher hardness compared to samples annealed for 5 min of soaking time, i.e., the sample having lower volume fraction of basal orientations.

5. Summary

The present study reveals the orientation-dependent hardness in annealed pure magnesium samples. It is observed that the basal orientations show a higher hardness value, and with increase in deviation from basal orientation the hardness value decreases.

The extent of texture formation in magnesium samples decreases with increase in soaking time of annealing when annealed at 200 °C. The volume fraction of basal orientations decreases till soaking time of 5 min which further increases on increasing the soaking time of annealing till 30 min. It is further observed that the microstructural developments are insignificant during annealing of magnesium samples for soaking time of 5 and 10 min, respectively. The present study confirms that the volume fraction of basal grains/orientations decides the bulk hardness of magnesium. Higher the volume fraction, greater is the hardness.

References

1. B.L. Mordike and T. Ebert, Magnesium: Properties—Applications—Potential, *Mater. Sci. Eng. A*, 2001, **302**, p 37–45
2. J. Xing, X. Yang, H. Miuna, and T. Sakai, Superplasticity of Magnesium Alloy AZ31 Processes by Severe Plastic Deformation, *Mater. Trans.*, 2007, **48**, p 1406–1411
3. T. Mukai, H. Watanabe, K. Ishikawa, and K. Higashi, Guide for Enhancement of Room Temperature Ductility in Mg Alloys at High Strain Rates, *Mater. Sci. Forum*, 2003, **419–422**, p 171–176
4. S.R. Agnew, P. Mehrotra, T.M. Lillo, G.M. Stoica, and P.K. Liaw, Texture Evolution of Five Wrought Magnesium Alloys during Route A Equal Channel Angular Extrusion: Experiments and Simulations, *Acta Mater.*, 2005, **53**, p 3135–3146
5. S. Sandlobes, S. Zaefferer, I. Schestakow, S. Yi, and R. Gonzalez-Martinez, On the Role of Non-basal Deformation Mechanisms for the Ductility of Mg and Mg-Y Alloys, *Acta Mater.*, 2011, **59**, p 429–439
6. S. Suwas, G. Gottstein, and R. Kumar, Evolution of Crystallographic Texture during Equal Channel Angular Extrusion (ECAE) and Its Effect on Secondary Processing of Magnesium, *Mater. Sci. Eng. A*, 2007, **471**, p 1–14
7. L. Capolungo, I.J. Beyerlein, and C.N. Tome, Slip-Assisted Twin Growth in Hexagonal Close-Packed Metals, *Scripta Mater.*, 2009, **60**, p 32–35
8. S.R. Agnew, J.A. Horton, and M.H. Yoo, TEM Invesitgation of Dislocation Structures in Mg and Mg-Li a-Solid Solution Alloys, *Metall. Mater. Trans. A*, 2002, **33**, p 851–858
9. M.H. Yoo and J.K. Lee, Deformation Twinning in h.c.p Metals and Alloys, *Philos. Mag. A*, 1991, **63**, p 987–1000
10. A. Jain and S.R. Agnew, Modeling the Temperature Dependent Effect of Twinning on the Behavior of Magnesium Alloy AZ31B Sheet, *Mater. Sci. Eng. A*, 2007, **462**, p 29–36
11. A. Chapuis and J.H. Driver, Temperature Dependency of Slip and Twinning in Plane Strain Compressed Magnesium Single Crystals, *Acta Mater.*, 2011, **59**, p 1986–1994
12. L.L. Chang, Y.N. Wang, X. Zhao, and J.C. Huang, Microstructure and Mechanical Properties in an AZ31 Magnesium Alloy Sheet Fabricated by Asymmetric Hot Extrusion, *Mater. Sci. Eng. A*, 2008, **496**, p 512–516
13. N. Stanford and M.R. Barnett, The Origin of "Rare Earth" Texture Development in Extruded Mg-Based Alloys and its Effect on Tensile Ductility, *Mater. Sci. Eng. A*, 2008, **496**, p 399–408
14. J. Koike, T. Kobayashi, T. Mukai, H. Watanabe, M. Suzuki, K. Maruyama, and K. Higashi, The Activity of Non-basal Slip Systems and Dynamic Recovery at Room Temperature in Fine-Grained AZ31B Magnesium Alloys, *Acta Mater.*, 2003, **51**, p 2055–2065
15. B. Beausir, S. Suwas, L.S. Tóth, K.W. Neale, and J.J. Fundenberger, Analysis of Texture Evolution in Magnesium During Equal Channel Angular Extrusion, *Acta Mater.*, 2008, **56**, p 200–214
16. S.H. Kim, B.S. You, C.D. Yim, and Y.M. Seo, Texture and Microstructure Changes in Asymmetrically Hot Rolled AZ31 Magnesium Alloy Sheets, *Mater. Lett.*, 2005, **59**, p 3876–3880
17. B. Beausir, S. Biswas, D. Kim, L.S. Toth, and S. Suwas, Analysis of Microstructure and Texture Evolution in Pure Magnesium During Symmetric and Asymmetric Rolling, *Acta Mater.*, 2009, **57**, p 5061–5077
18. X. Gong, H. Li, S.B. Kang, J.H. Cho, and S. Li, Microstructure and Mechanical Properties of Twin-Roll Cast Mg-4.5Al-1.0Zn Sheets Processed by Differential Speed Rolling, *Mater. Des.*, 2010, **31**, p 1581–1587

19. S.E. Ion, F.J. Humphreys, and S.H. White, Dynamic Recrystallization and the Development of Microstructure During the High Temperature Deformation of Magnesium, *Acta. Mater.*, 1982, **30**, p 1909–1919

20. Y. Qiao, X. Wang, Z. Liu, and E. Wang, Effect of Temperature on Microstructures, Texture and Mechanical Properties of Hot Rolled Pure Mg Sheets, *Mater. Sci. Eng. A*, 2013, **568**, p 202–205

21. K. Pawlik and P. Ozga, LaboTex: The Texture Analysis Software, Göttinger Arbeiten zur Geologie und Paläontologie, SB4, 1999

22. I. Groma and F. Szekely, Analysis of the Asymptotic Properties of X-ray Line Broadening Caused by Dislocations, *J. Appl. Cryst.*, 2000, **33**, p 1329–1334

23. N. Rajmohan, Y. Hayakawa, J.A. Szpunar, and J.H. Root, Neutron Diffraction Method for Stored Energy Measurement in Interstitial Free Steel, *Acta Mater.*, 1997, **45**, p 2485–2494

24. T. Mura, *Micromechanics of Defects in Solids*, Matrinus Nijhoff Publishers, Dordrecht, 1987, p 421–439

25. Z. Zeng, Y. Zhang, and S. Jonsson, Microstructure and Texture Evolution of Commercial Pure Titanium Deformed at Elevated Temperatures, *Mater. Sci. Eng. A*, 2009, **513–514**, p 83–90

26. T.B. Britton, H. Liang, F.P.E. Dunne, and A.J. Wilkinson, The Effect of Crystal Orientation on the Indentation Response of Commercially Pure Titanium: Experiments and Simulations, *Proc. R. Soc. A*, 2010, **466**, p 695–719

27. G.B. Viswanathan, E. Lee, D.M. Maher, S. Banerjee, and H.L. Fraser, Direct Observations and Analyses of Dislocation Substructures in the α Phase of an α/β Ti-Alloy Formed by Nanoindentation, *Acta Mater.*, 2005, **53**, p 5101–5115

28. F.K. Mante, G.R. Baran, and B. Lucas, Nanoindentation Studies of Titanium Single Crystals, *Biomaterials*, 1999, **20**, p 1051–1055

29. G. Nayyeri, W. J. Poole and C. W. Sinclair, *Proc. 9th Int. Conf. Mg Alloys Appl.*, eds. W. J. Poole and K. U. Kainer, Vancouver, 2012, p 1325–1330

30. R. Sanchez-Martin, M.T. Perez-Prado, J. Segurado, J. Bohlen, I. Gutierrez-Urrutia, J. Llorca, and J.M. Molina-Aldareguia, Measuring the Critical Resolved Shear Stresses in Mg Alloys by Instrumented Nanoindentation, *Acta Mater.*, 2014, **71**, p 283–292

31. B. Selvarajou, J.H. Shin, T.K. Ha, I. Choi, S.P. Joshi, and H.N. Han, Orientation-Dependent Indentation Response of Magnesium Single Crystals: Modeling and Experiments, *Acta Mater.*, 2014, **81**, p 358–376

32. H. Yoshinaga and R. Horiuchi, Deformation Mechanism in Magnesium Single Crystals Compressed in the Direction Parallel to Hexagonal Axis, *Trans. JIM*, 1963, **4**, p 1–8

33. M.R. Barnett, Twinning and the Ductility of Magnesium Alloys: Part I, "Contraction" Twins, *Mater. Sci. Eng. A*, 2007, **464**, p 1–7

34. M.R. Barnett, Twinning and the Ductility of Magnesium Alloys: Part II, "Contraction" Twins, *Mater. Sci. Eng. A*, 2007, **464**, p 8–16

35. L. Meng, P. Yang, Q. Xie, and W. Mao, Analyses on Compression Twins in Magnesium, *Mater. Trans.*, 2008, **49**, p 710–714

36. S. Biswas, S.S. Dhinwal, and S. Suwas, Room-Temperature Equal Channel Angular Extrusion of Pure Magnesium, *Acta Mater.*, 2010, **58**, p 3247–3261